Downloaded from SAE International by University of Wisconsin - Madison , Monday, July 06, 2020

2020-01-0160 Published 14 Apr 2020

An Analytical Approach for Calculating Instantaneous Multilayer-Coated Wall Surface Temperature in an Engine

G. Koutsakis and J.B. Ghandhi University of Wisconsin Madison

Citation: Koutsakis, G. and Ghandhi, J.B., "An Analytical Approach for Calculating Instantaneous Multilayer-Coated Wall Surface Temperature in an Engine," *SAE Int. J. Advances & Curr. Prac. in Mobility* 2(3):1303-1313, 2020, doi:10.4271/2020-01-0160.

This article is from WCX™ 2020 SAE World Congress Experience.

Abstract

Thermal swing coatings that have low volumetric heat capacity and low thermal conductivity are attractive because they have the potential to significantly reduce heat transfer to the combustion chamber walls. This paper presents an analytical method for determining the exact solution of the time-resolved wall temperature during the engine cycle for any number of coating layers and properties using the Laplace transformed heat diffusion equation. The method relies only on material properties and the past heat flux history, and represents the exact solution of the heat diffusion equation. The analytical nature of the solution enables fast computation and, therefore, application to system-level optimization calculations. The model relies on an assumption of one-dimensional heat flow, and constant material properties. The major advantage of this approach compared to the standard finite difference approach, wherein the wall is finely discretized, is that there is no approximation and the accuracy is guaranteed, *i.e.,* it does not depend on nodal density. Results are presented for both a quasi-steady operating condition and for an engine transient event. In the latter case a 200-fold reduction in computation time relative to a finite difference code was realized.

Introduction

Climate change concerns drive government environmental agencies to set stringent emission regulations for engine manufacturers, making the design process more and more challenging due to the trade-off between pollutant emissions and engine efficiency. A pathway to achieve higher efficiency is to reduce the heat transfer losses to the combustion chamber walls. Depositing insulating coatings on the combustion chamber surfaces is a relatively old concept, but recent materials having low thermal conductivity and low volumetric heat capacity properties have renewed the interest of the engine community.

Initial simulations and experiments in reciprocating engines were conducted using thermal barrier coating (TBC) materials developed for gas turbine applications. A typical structure consisted of a bond coat, typically made of NiCrAlY alloy, and a top coat of yttria stabilized zirconia (YSZ) or silicon nitride (Si_3N_4). The effective coating properties (including contact resistances and bond coat) had lower thermal conductivity (~1 vs. ~100 $Wm^{-1}K^{-1}$) and almost equivalent volumetric heat capacity (~2.5 MJ m^{-3} K^{-1} vs. ~3.0 MJ m^{-3} K^{-1}) compared to the base engine wall.

The thermodynamic performance and pollutant emissions results of TBC engines varied widely. Researchers have investigated the effect of YSZ as a TBC material deposited onto metal engine wall components in various thicknesses and different engine operating conditions/configurations. Improved fuel economy [1, 2, 3] was observed by some researchers while others reported inferior performance results [4, 5, 6, 7, 8] with TBCs. Experimental and modeling work from Morel *et al.* [9] found reduced fuel consumption for every coated case tested compared to an uncoated baseline. Dickey *et al.* [7], however, found efficiency gain from simulation results, but their experimental studies showed a decrease in thermal efficiency due, in part, to non-re-optimization of combustion after the TBC addition.

Air-gapped monolithic ceramics and low thermal conductivity metal alloys [10, 11, 12, 13] have also been investigated for potential efficiency increase. Fuel consumption decreased for a fully ceramic [10] and metal [11] air-gapped insulated uncooled single-cylinder diesel engine, although a similar setup to [10] reported higher fuel consumption [13].

To get the full benefit out of a coated engine, combustion system re-optimization [6, 9, 11, 14], *e.g.* fuel injection timing, injection rates and pressures, air intake temperature and exhaust pressure, is necessary when compared to the baseline. A number of previous experiments (without any combustion parameter re-optimization) have shown degraded combustion [7, 8, 15, 16] for diesel engines with TBCs. This deterioration may be ascribed to slower combustion, *i.e.*, less premixed burn fraction and increased diffusion burn duration for the insulated engine, reducing thermal efficiency [7]. Additionally, direct substitution of coated components without re-optimization leads to excess soot deposits on piston surface [8], fuel injector malfunctioning in hotter combustion chamber temperatures [14] and thermal boundary layer thinning due

Downloaded from SAE International by University of Wisconsin - Madison , Monday, July 06, 2020

to elevated wall temperatures [15]. In the latter, Woschni *et al.* [15] argued that the local heat transfer coefficient increased substantially and counter-balanced any heat transfer benefit that would have occurred with in-cylinder TBCs. On the other hand, promising results in fuel economy were presented after re-optimizing the combustion system [6, 9, 11], but some authors suggested more fundamental redesign is required [8].

Heat flux magnitudes in combustion surfaces vary significantly temporally and spatially. A non-coated heavy-duty diesel engine at high load conditions can reach a peak heat flux of 10 MW/m^2 [17] near the combustion event. During the intake stroke, heat typically flows from the engine walls to the inducted air during the intake valve opening increasing the temperature and thus decreasing intake charge density. For a TBC combustion chamber wall, temperatures are increased and thus there is higher negative heat flux during that part of the stroke. Decreased volumetric efficiency [1, 7, 13] does not necessarily imply that the overall system efficiency is negatively impacted.

In-cylinder heat transfer on insulated/TBC engines has been investigated. A number of researchers claimed that the nature of the heat transfer process remained unchanged throughout the cycle due to the coating addition, and the lower difference between gas and the wall temperature reduces heat flux, $\dot{q}'' \equiv h(t_g - t_w)$, where h is the convection coefficient, t_g and t_w is the gas and wall temperature. Several studies [1, 8, 11, 18] agreed with this hypothesis. Conversely, a handful of others [13, 15, 16] state that although increased cylinder wall temperature is a benefit, the convection coefficient becomes large enough to overcome the temperature difference benefit and, thus, the heat flux actually rises.

The potential of the heat loss reduction to increase brake work is not realized for every coating and engine configuration. Some studies have found [1, 7, 8, 16, 19] that the majority of the heat ended up in the exhaust as sensible enthalpy while others [2, 3, 13] observed lower exhaust temperatures. Depending on the application, an increase in exhaust enthalpy might favor the overall system efficiency, for example, additional work might be produced by turbo-compounding the engine, additional fueling needed for cold-start after-treatment heating time may be reduced [20], the enthalpy may be used by waste heat recovery systems [21], or high residual temperatures may enable low temperature combustion strategies at low load conditions.

Thermal-swing coatings having low thermal conductivity and low volumetric heat capacity (mainly driven by high porosity), were recently proposed for in-cylinder heat insulation [22]. This combination of properties, allows the surface wall temperature to track the gas temperature closer, reducing the wall heat transfer throughout the cycle. A silica reinforced porous anodized aluminum (SiRPA) coating developed by Toyota, showed lower fuel consumption and higher cold-start efficiency [23]. Durrett *et al.* [24] have developed a coating with similar thermal properties made of sintered hollow nickel-alloy micro-spheres to achieve higher porosity. Reliable operation in a spark-ignited engine environment was demonstrated by Andrie *et al.* [25] using a high volume low pressure (HVLP) method; two coatings with outstanding coating properties were developed. The new generation of thermal-swing coatings typically have thermal conductivity about one quarter of zirconia and volumetric heat capacity around one third of zirconia.

Finite difference solutions have been used to predict the wall surface temperatures of combustion chambers. The relatively thin coatings and the short time scales compared to the engine wall, however, require high density nodal discretization near the surface to guarantee numerical stability and accuracy [26, 27]. Earlier studies used thermal network models [28, 29, 30, 31, 32], but these can effectively be considered very low-fidelity finite difference methods. Cycle-resolved transient wall surface temperature, limited just to a two-layer wall, using Fourier analysis [33] requires at least an entire cycle worth of information to calculate the coefficients from the gas temperature of the previous cycle and therefore estimate wall temperature and heat transfer rate. A proper in-cylinder coating design requires optimization of the entire engine system, including the full exhaust after-treatment system, which can only be achieved using sophisticated, commercially available codes. Implementing such finite difference models or cycle-resolved equation in conjunction with these code makes the calculation time consuming.

The objective of this work is to provide a tool to be used by engine designers to accurately predict the surface temperature of multi-layer thermal barrier coated walls. The proposed methodology can be coupled with existing commercial cycle simulation codes to determine the overall wall heat transfer rate. The only inputs that the method requires are the material properties and the past heat flux history. The analytical nature of the solution enables fast computation to allow transient system-level optimization calculations.

Mathematical Model

Consider thermal diffusion in a solid 1-D multi-layer wall with overall thickness L and constant thermophysical properties, as shown in Fig. 1. Any number of layers is allowable. The governing heat diffusion equation is

$$k\frac{\partial^2 t}{\partial x^2} = \rho c \frac{\partial t}{\partial \theta} \tag{1}$$

FIGURE 1 Illustration of an 1D multi-layer engine wall. Boundary condition from the combustion chamber side is assumed to be heat flux, while from the coolant side constant temperature.

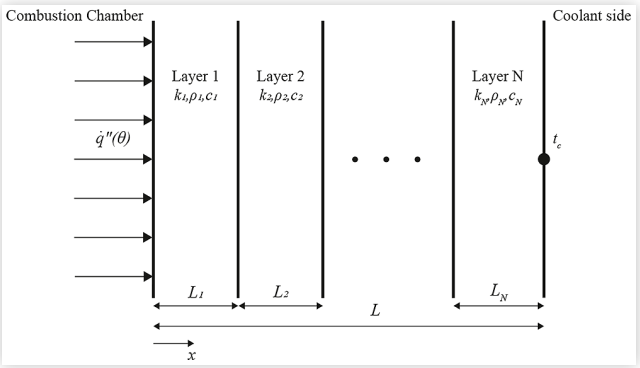

© SAE International.

Downloaded from SAE International by University of Wisconsin - Madison , Monday, July 06, 2020

where t is temperature, θ is time, k and ρc are thermal conductivity and volumetric heat capacity, respectively. The $x = 0$ location represents the gas-side surface where a time-varying heat flux, $\dot{q}''(\theta)$, is imposed

$$-k\frac{\partial t}{\partial x}\bigg|_{x=0} = \dot{q}''(\theta) = f(\theta) \tag{2}$$

A heat flux boundary condition is used instead of a convective boundary because both the gas temperature and heat transfer coefficient change with time in an engine.

The initial condition is a uniform wall temperature, but the applied heat flux is periodic in a reciprocating-engine and one is often interested in the converged periodic solution. For this case, the temperature at $x = L$ is constant and, for simplicity, can be taken as equal to the coolant temperature, t_c,

$$t_{x=L,\theta\to\infty} = t_c \tag{3}$$

It will be shown that a convective backside boundary condition can also be implemented with no change in procedure.

In order to solve the problem with an arbitrary input heat flux, the linearity of the problem will be exploited and the final solution will be the sum of the solutions to a series of step changes in heat flux applied to the wall. The surface temperature will therefore be the result of all previous step inputs, and the step inputs will be based on a discretization of the heat flux in time. The treatment required to use the converged periodic solution as the initial condition will be discussed below.

In order to use the superposition method, the problem statement needs to change slightly. At the initial time the wall temperature is uniform and with no loss of generality can be taken as zero.

$$t_{x,\theta=0} = 0 \tag{4}$$

The initialization and back-side boundary condition treatment are discussed below. The solution to the multi-layer, 1-D wall conduction problem subject to a step change in heat flux can be found using the methodology established initially by Pipes [34] and later by Carslaw and Jaeger [35]. The solution is achieved by taking the Laplace transform of Equation (1). A detailed derivation of the proposed problem has been solved for internal combustion engine applications in [37]. Using the notation $\hat{t}_o$ as the Laplace transform of gas-side surface temperature, and likewise $\hat{q}_o$ as the Laplace transform of surface heat flux, one can write for any number of layers

$$\begin{bmatrix} \hat{t}_o \\ \hat{q}_o \end{bmatrix} = \begin{bmatrix} A & B \\ C & D \end{bmatrix} \begin{bmatrix} \hat{t}_N \\ \hat{q}_N \end{bmatrix} \tag{5}$$

where N is the number of layers; $\hat{t}_N$ and $\hat{q}_N$ are the transform of t and $\dot{q}''$ at the coolant side. The coefficients of the matrix in (5) define the *overall* transfer matrix, which is comprised of the product of transfer matrices for each individual layer

$$\begin{bmatrix} A & B \\ C & D \end{bmatrix} = \begin{bmatrix} A_1 & B_1 \\ C_1 & D_1 \end{bmatrix} \cdot \begin{bmatrix} A_2 & B_2 \\ C_2 & D_2 \end{bmatrix} \cdots \begin{bmatrix} A_N & B_N \\ C_N & D_N \end{bmatrix} \tag{6}$$

The transfer matrix for each layer is given by [34]

$$\begin{bmatrix} A_i & B_i \\ C_i & D_i \end{bmatrix} = \begin{bmatrix} \cosh\sqrt{sR_iC_i} & \dfrac{R_i}{\sqrt{sR_iC_i}}\sinh\sqrt{sR_iC_i} \\ \dfrac{\sqrt{sR_iC_i}}{R_i}\sinh\sqrt{sR_iC_i} & \cosh\sqrt{sR_iC_i} \end{bmatrix} \tag{7}$$

where s is the Laplace domain frequency, R_i is the thermal resistance of layer i given by

$$R_i = \frac{L_i}{k_i} \tag{8}$$

and C_i is the volumetric heat capacity per unit area for layer i.

$$C_i = L_i\rho_i c_i \tag{9}$$

Using this formulation, a contact resistance can be represented as

$$\begin{bmatrix} A_i & B_i \\ C_i & D_i \end{bmatrix} = \begin{bmatrix} 1 & R_i \\ 0 & 1 \end{bmatrix} \tag{10}$$

which follows from (7) when the heat capacity is negligible compared to the resistance. Likewise, a convective boundary condition having a convective heat transfer coefficient, h, can be represented as

$$\begin{bmatrix} A_i & B_i \\ C_i & D_i \end{bmatrix} = \begin{bmatrix} 1 & \dfrac{1}{h} \\ 0 & 1 \end{bmatrix} \tag{11}$$

The overall transfer matrix of the multi-layer wall given by (6) can be recast in a manner that takes advantage of the known boundary conditions $\hat{t}_N$ (ultimately at $x = L$) and $\hat{q}_o$, which is the prescribed input, to get

$$\begin{bmatrix} \hat{t}_o \\ \hat{q}_N \end{bmatrix} = \frac{1}{D} \cdot \begin{bmatrix} 1 & B \\ -C & 1 \end{bmatrix} \begin{bmatrix} \hat{t}_N \\ \hat{q}_o \end{bmatrix} \tag{12}$$

This set of equations relates only information on the surface boundaries, *i.e.* at $x = 0, L$, but it is the exact solution of the governing partial differential equation. Further, using the fact that $\hat{t}_N = 0$, and by applying a step impulse of heat flux with unity magnitude such that $\hat{q}_o = \mathbf{1} \cdot \frac{1}{s}$ (where $\frac{1}{s}$ is the Laplace transform of a step change) the above formula simplifies to

$$\hat{t}_o = \mathbf{1} \cdot \frac{1}{s} \cdot \frac{B}{D} \tag{13}$$

The inversion from the Laplace frequency domain to the time domain is the last step required to solve for the wall surface temperature as a function of time. Utilizing the general formula of the inverse Laplace transform, one gets

$$t_o(\theta) = \mathbf{1} \cdot \frac{1}{2\pi j} \int_{\Omega - j\infty}^{\Omega + j\infty} \frac{1}{s} \cdot \frac{B}{D} e^{s\theta} ds \tag{14}$$

where $j = \sqrt{-1}$ and the constant Ω is a large positive real number approaching infinity.

Inverse transforms of this kind are neither listed in standard tables nor given by computer software packages (even for a two-layer problem). In complex analysis, the

Downloaded from SAE International by University of Wisconsin - Madison , Monday, July 06, 2020

residue theorem provides a powerful tool to evaluate integrals, *i.e.*, the inverse Laplace transform in this case [36]. A complete derivation of this inversion can be found in [37] along with an analytical solution for the limit of negligible coating thermal inertia.

The residue theorem gives the result that the integral of Equation (14) can be found as $2\pi j$ times the sum of the residues of the integrand, which are found when the integrand has indeterminate value. The locations of indeterminate integrand are also referred to as the poles. There is a simple pole at $s = 0$ and a series of poles where $D(s) = 0$. Carlslaw and Jaeger [35] have shown for a different boundary condition problem that the zeros of the matrix coefficient lie on the negative real axis. Relatively simple numerical techniques can be used to find the values $s = -\beta_m$, where $m = 1, 2 \ldots \infty$, that are zeros of $D(s)$. The choice of $s = -\beta$ for the root calculation procedure [38] is made in order for β to be a real positive number. Invoking the assumption that the poles lie on the negative real axis, then Eq. (7) becomes

$$\begin{bmatrix} A_i & B_i \\ C_i & D_i \end{bmatrix} = \begin{bmatrix} \cos\sqrt{\beta R_i C_i} & \frac{R_i}{\sqrt{\beta R_i C_i}} \sin\sqrt{\beta R_i C_i} \\ \frac{-\sqrt{\beta R_i C_i}}{R_i} \sin\sqrt{\beta R_i C_i} & \cos\sqrt{\beta R_i C_i} \end{bmatrix} \quad (15)$$

Recall, that in this form the values of β are positive. Finally, after some manipulation and application of the superposition principle [37], the wall surface temperature at time θ_n is given, as

$$t_o(\theta_n) = t_c + \left(\bar{q}'' + \sum_{i=0}^{n} \Delta \dot{q}_i'' \right) R_{total} - \sum_{i=0}^{n} \Delta \dot{q}_i'' \cdot g(\theta_n - \theta_i) \quad (16)$$

where the response factor, $g(\theta_n - \theta_i)$, describes the decay of the effect of the step change in heat flux that occurred from time i to time n and is given by

$$g(\theta_n - \theta_i) = \sum_{m=1}^{\infty} \frac{B|_{s=-\beta_m}}{\beta_m \left. \frac{dD(s)}{ds} \right|_{s=-\beta_m}} e^{-\beta_m(\theta_n - \theta_i)} \quad (17)$$

$\Delta \dot{q}_i'' = (\dot{q}_i'' - \dot{q}_{i-1}'')$ is the discretized heat flux at the wall surface, and the values of B and $\frac{dD}{ds}$ are determined numerically at the poles $s = -\beta_m$. R_{total} is the sum of the resistances of all of the layers, $\sum R_i$. Note that if one is using (7) then the value of s (which is a negative real number) should be used, whereas when using (15) the value of β (which is a positive real number) should be used.

The first term of Equation (16) imposes the backside wall temperature boundary condition, and the second provides an initial condition that takes into account the converged steady solution of the wall subjected to a periodic condition having a net mean heat flux $\bar{q}''$. This considerably shortens the time needed to reach steady state, and is widely employed in finite difference solutions. In addition, the summation for the last term of (16) starts at zero even though this would require knowing heat flux at negative time. This is done to account for the transient effect of effectively removing the mean heat flux that led to the second term in (16), see [37] for details. Thus, the zeroth element of $\Delta q''$ needs to be set as $\Delta q_0'' = -\bar{q}'' + \dot{q}_0''$. In the limit of long times in the past, the response factor g converges to zero - as this will be evident later, so the net effect is that the second and third terms becomes zero.

Response Factor

The response factor, g, in (17) is the summation of the product of a fraction that is purely material/structure dependent and an exponential term that depends on both structure and the lapsed time interval. The roots or poles, β_m, which are the locations were $D(s) = 0$, have the same nature as eigenvalues, therefore it is important that none are missed. In practice, the response factor can be precalculated and tabulated *a priori* provided that the time step of the simuluation where it will be used is known.

Two test cases will be shown by way of demonstration. The first case represents a state-of-the-art thermal-swing type of coating [25] referred to hereafter as the TS case. The second case represents a four-layer wall that consisted of a traditional yttria-stabilized zirconia (YSZ) coating, a gradient layer, and a bond coat [39]. The thermophysical properties and coating thicknesses are shown in Table 1. In both cases the engine wall was aluminum [40] and the total domain length remained fixed at 5mm.

The first 15 roots were calculated for both cases. Figure 2 (top), shows the corresponding function $D(s)$ for the TS coating, with the roots of the equation marked on the x axis. Likewise, Fig. 2 (bottom), shows the results for the YSZ coating. It is seen that the roots of $D(s) = 0$ (indexed as m) are sequentially (and substantially) more negative as m increases - note that Fig. 2 uses the square root of β_m on the abscissa. Therefore the terms of the summation over m diminish in importance due to the exponential term at large m. Additionally, $D(s)$ is seen to oscillate and some roots are located very close to one another. For the two test cases illustrated above, the first 15 roots of $D(s) = 0$ are given in Table 3 and in the Appendix. The number of roots required for accuracy depends on many factors, but in general the goal is to find the minimum number to save computational cost (again, this is pre-computed so computational time is not too important). The fraction in the summation is useful for assessing whether one has found all of the roots, *i.e.*, roots have not been missed if they are close together such as the 4th and 5th root in Fig. 2 for both the two- and four-layer wall. It is required that

$$\sum_{m=1}^{\infty} \frac{B|_{s=-\beta_m}}{\beta_m \left. \frac{dD(s)}{ds} \right|_{s=-\beta_m}} \simeq R_{total} \quad (18)$$

TABLE 1 Material properties of coatings and engine wall; units are J - m - K - s.

	k	ρc	L
TS	0.35	0.4×10^6	100×10^{-6}
YSZ	0.77	1.8×10^6	210×10^{-6}
Gradient	0.85	1.5×10^6	70×10^{-6}
Bond	4.07	0.9×10^6	70×10^{-6}
Aluminum	123	2.8×10^6	(bal. for 5mm)

© SAE International.

Downloaded from SAE International by University of Wisconsin - Madison , Monday, July 06, 2020

FIGURE 2 *D*(*s*) with zeros identified for a two-layer (top) and four-layer (bottom) cylinder engine wall

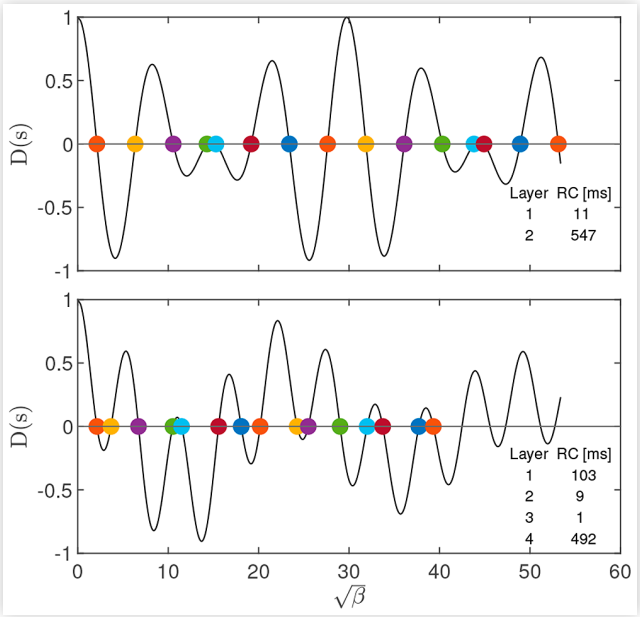

© SAE International.

in a steady-state limiting case. By defining a suitable error criteria, one can assess whether all of the roots have been found.

Assuming that all of the roots have been found, then this term can also be used to assess how many roots are required for maintaining sufficient accuracy. There is an infinite set of β_m's and all of them should be included for complete accuracy. For practical purposes, the question that arises is how large a root β_m must be before it can be neglected (due to the vanishing nature of the exponential term). For a cut-off root, β_{max}, it can be seen from (17) that the contribution of the β_{max} is at most $e^{-\beta_{max}\Delta\theta}$ where $\Delta\theta$ is the timestep. To ensure a precision of 5×10^{-5} one can neglect contribution from those roots for which

$$e^{-\beta_{max}\Delta\theta} < 5\times10^{-5} \simeq e^{-10} \tag{19}$$

or

$$\beta_{max} \cdot \Delta\theta > 10 \tag{20}$$

The response functions for the TS and YSZ coating are shown in Fig. 3. The plot abscissa was chosen to emphasize the fact that the response factor represents the importance of *previous* heat flux events on the *current* surface temperature. The response factor was calculated using 100 roots and a time step of 0.128ms, which corresponds to 1 crank angle at 1300 rpm. Under these conditions, the TS β_{100} root and the first time step give a value of 17.33 in (20), suggesting excellent accuracy from the first step. The response curves for the two cases are both seen to monotonically decrease with lapsed time, which indicates that the effect of a heat flux event dies out in time. The two curves start at a different point on the ordinate because the first value corresponds to R_{total}, which is different for the two cases.

FIGURE 3 Response factor *g* as a function of negative time for a two-layer TS and a four-layer YSZ coating. The total time shown corresponds to 10 cycles at 1300 rpm.

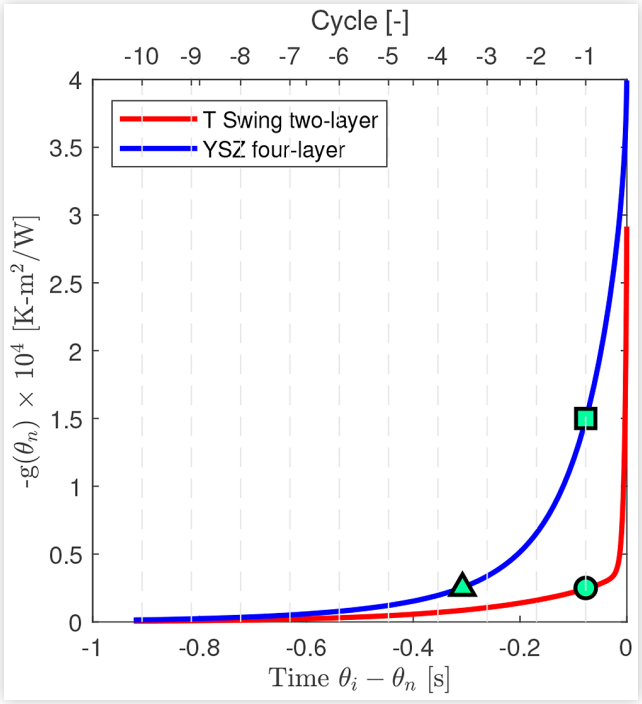

© SAE International.

The major difference between the two curves is the rapid initial change of the TS coating response followed by a more slowly decreasing tail, whereas the YSZ coating has a more sustained decaying response. This behavior is driven by the large difference in time scales for the TS coating and base wall; for the YSZ coating the time scales are much closer. The overall time required to achieve an atttenuation of the response function that is 10% of the initial value is equivalent to slightly less than 0.5 cycles at 1300 rpm for the TS coating and 2.5 cycles for the YSZ coating.

Figure 3 embodies all of the conduction physics of the problem, and it should be used as a guide when coating design in engines is undertaken. Consider the steady operating case where the heat flux is the same every cycle as an example. The contribution of the last cycle on the surface temperature for the TS coating has attenuated by ≃90%, see the circle in Fig. 3. In comparison, for the YSZ coating, the attenuation is much less, only ≃60% as denoted by the square. In order to achieve a similar attenuation between the TS coating at one cycle, one needs to wait 3.5 cycles with the YSZ coating, shown by the triangle in Fig. 3. Alternatively, the TS coating *forgets* the majority of the contribution of a heat flux event within one cycle at 1300 rpm, but it takes the YSZ coating 3.5 cycles to forget the same heat flux event.

Demonstration

A simple model was constructed to demonstrate the coated wall temperature solution methodology. The engine model is

Downloaded from SAE International by University of Wisconsin - Madison , Monday, July 06, 2020

crude, but suffices for the demonstration of the wall temperature calculation. A closed-cycle (from IVC to EVO) single-zone model was created with the chemical kinetics solver Cantera in Python [41]. The cylinder contents are uniform throughout the combustion chamber. Fuel was added to the system at a mass flow rate that was prescribed by a Wiebe function with the parameters tuned to match data provided by John Deere. Ignition and combustion were calculated directly using a 45 species / 155 reaction kinetic mechanism [42]. The model fuel was *n*-heptane.

Convective heat transfer to the wall is given as

$$\dot{q}'' = h\left(t_g - t_w\right) \tag{21}$$

where h is the heat transfer coefficient, t_g is the bulk gas temperature from the gas-phase kinetics solver and t_w is the coated wall temperature. According to literature cited in the Introduction, the heat transfer coefficient can significantly be altered in a coated engine. In this work, the effect of the coating on the heat transfer coefficient was not included. The heat transfer coefficient was calculated according to the Annand correlation [43]

$$h = C\frac{k}{B}Re^{0.7} \tag{22}$$

where C is a constant coefficient taken as 0.5, k is the charge conductivity, B is the cylinder bore and Re is the Reynolds number

$$Re = \frac{\rho \bar{S}_p B}{\mu} \tag{23}$$

where ρ and μ are the air density and dynamic viscosity, respectively, $\bar{S}_p$ is the mean piston speed, and B as the cylinder bore.

The open portion of the cycle was modeled in three parts. First, the gas temperature was linearly interpolated between EVO and BDC from the EVO temperature to the temperature arising from an isentropic expansion from the EVO state to the exhaust pressure. Second, during the exhaust stroke until gas-exchange TDC, the gas temperature remained constant. Finally, from TDC until 30° aTDC, during the filling process, the gas temperature dropped linearly to the IVC temperature where it remained constant until IVC. The heat transfer coefficient remained constant at 400 W/m^2-K during the open part of the cycle.

The full model solution requires time-resolved wall temperature data. This can be time consuming, however, if it is embedded in the combustion simulation, which is why a fast analytical method is desired. Many past researchers have used an iterative approach wherin the combustion simulation was performed with a prescribed time-varying wall temperature, then the wall model was run; the results of the wall model are then used in the following cycle's combustion simulation; the process is repeated until a convergence criteria is satisfied. The present model can be used in this manner if desired. But, the model was implemented here in a way that the wall temperature was calculated for every time step of the combustion simulation in order to allow transient simulations.

Engine Model Comparison

Data from two engine conditions were provided by John Deere for the 4045 engine geometry, see Table 2. The first case, referred to hereafter as the low load case, was 7.2 bar IMEPg at 1300 rpm. The second case, referred to hereafter as the high load case, was 17.2 IMEPg bar again at 1300 rpm.

The closed-cycle cylinder pressure was approximated with the Cantera code. A comparison of the model pressure to the data provided by John Deere is shown in Figure 4 (top). Overall, it can be seen that there is good agreement for the closed-cycle period using the relatively simple model. The bulk gas temperature, see Fig. 4 (bottom), also matches the John Deere data quite well during the closed portion of the cycle.

TABLE 2 John Deere 4045 engine geometry

Displacement volume / cylinder	1.125 cc
Stroke	127 mm
Bore	106.5 mm
Connecting Rod	203 mm
Compression Ratio	17.0:1
Intake Valve Close	-154° aTDC
Exhaust Valve Open	126° aTDC
Coolant temperature	373 K

© SAE International.

FIGURE 4 Pressure (top) and gas temperatures (bottom) traces as a function of crank-angle. Matching conditions between UW-Cantera and John Deere low and high load test cases.

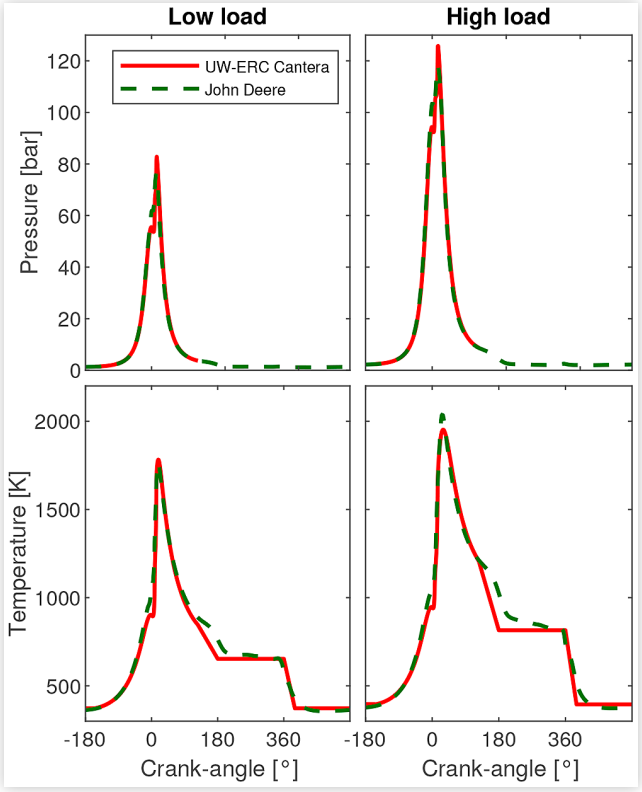

© SAE International.

Downloaded from SAE International by University of Wisconsin - Madison , Monday, July 06, 2020

The approximations of the open portion of the cycle are also, for the present purposes, seen to be sufficient.

Quasi-Steady Simulation

The low load scenario was chosen to illustrate the quasi-steady solution. The following cases are compared: (1) a one-layer aluminum wall of 5 mm thickness, (2) a two-layer, TS-coated aluminum wall, and (3) a four-layer, YSZ coated aluminum wall. The coating material thermal properties and layer thicknesses are described above in Table 1. The response factors for the test cases were calculated using 100 roots. A temperature difference was calculated between the current and previous cycle's value, and when an absolute convergence criteria of wall temperature difference of 0.05K (maximum over a cycle) was reached, the simulation ended.

As expected, the wall temperature solutions required some number of cycles to converge, mostly due to the contribution of the initial step $-\bar{q}''$ decay and the volumetric heat capacity of the multi-layer structure.

In Fig. 5, the one-layer aluminum wall (black) results in an almost negligible temperature swing [44], and took five (5) cycles to fully converge. The four-layer YSZ (blue) case required four (4) cycles to converge. The combination of low thermal conductivity and high volumetric heat capacity of the structure led to a significantly elevated cycle-average wall temperature, which may be detrimental for engine applications. Finally, the two-layer TS case (red) needed only two (2) cycles for complete convergence. The low thermal conductivity and low volumetric heat capacity of the coating makes the results promising because the wall temperature follows the gas temperature much closer.

Transient Simulation

As discussed above, the high accuracy and low computational cost associated with this method make it well suited for transient analysis. A transient simulation scenario of a load step change is illustrated below. The simulation was for a load step change at a constant speed of 1300 rpm using the John Deere 4045 engine. The first 10 cycles were at the low load condition, and the 11th and all subsequent cycles were at the high load condition, refer to Fig. 4 for operating details. Both the TS and YSZ coating structures described above were simulated.

Results of the simulation are shown in Fig. 6. For each coating, only three cycles of the simulation are shown: cycle 10 - the last low-load cycle (dashed), cycle 11 - the first high-load cycle (open circles), and cycle 100 - the final cycle (solid).

Consider first the TS coating results. Due to its low-volumetric heat capacity, the TS coating (red) required very little time to respond fully to the sudden load step change. This can be seen by how closely cycle 11 matches the final cycle of the simulation, which is essentially the fully converged solution for operation at the high load condition. It is also interesting to note that the wall temperature during the intake stroke is, at the scale of Fig. 6, independent of engine load. This is the manifestation of the very rapid decrease in the response factor with time for the TS coating that is seen in Fig. 3, *i.e.*, there is very little memory of the past heat flux events.

FIGURE 5 Coated surface wall temperature for the low load scenario of the converged cycle for an one-layer aluminum wall (black), a two-layer TS coating (red) and a four-layer YSZ coating (blue).

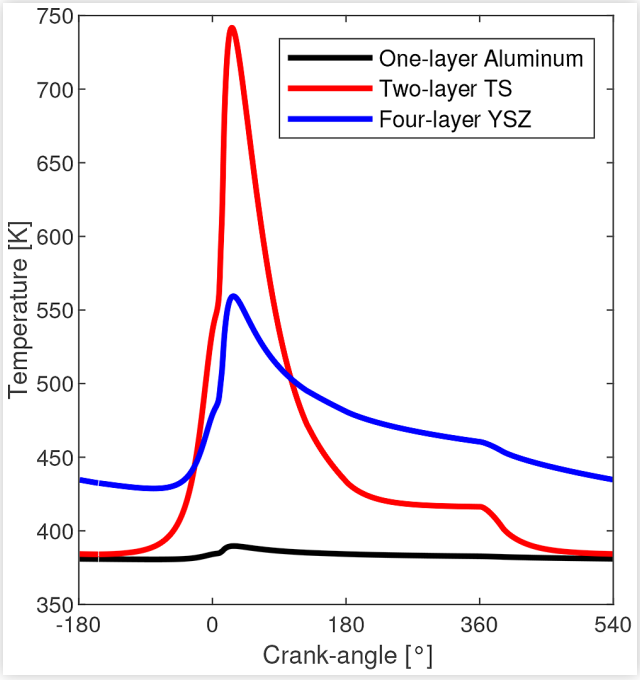

© SAE International.

FIGURE 6 Transient simulation results of the coated wall surface temperature for 100 cycles. Cycle 10 (dashed) is the last low load cycle, cycle 11 is the first high load (circle) cycle, cycle 100 is the last high load (solid) cycle. The two-layer TS coating (red) results are shown at left and the four-layer YSZ coating (blue) results are at right.

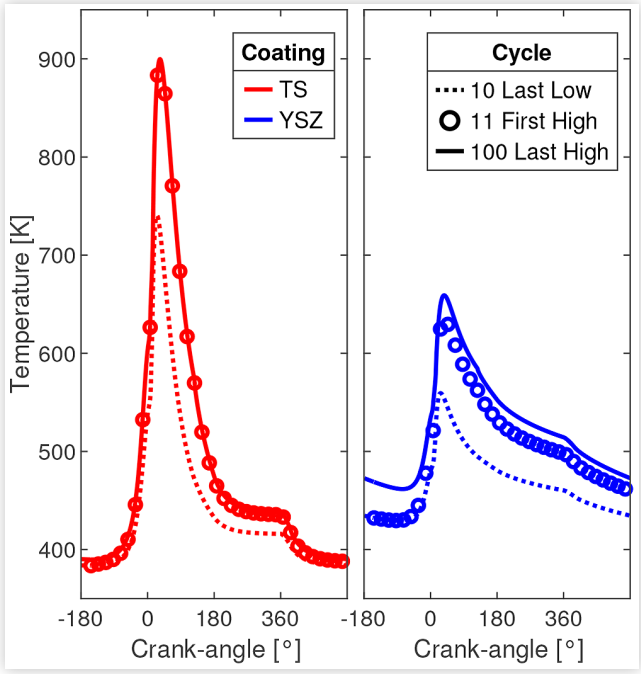

© SAE International.

Downloaded from SAE International by University of Wisconsin - Madison , Monday, July 06, 2020

FIGURE 7 Coated wall temperature at BDC for the 100 cycle transient simulation, for the two-layer TS coating (red) and the four-layer YSZ coating (blue)

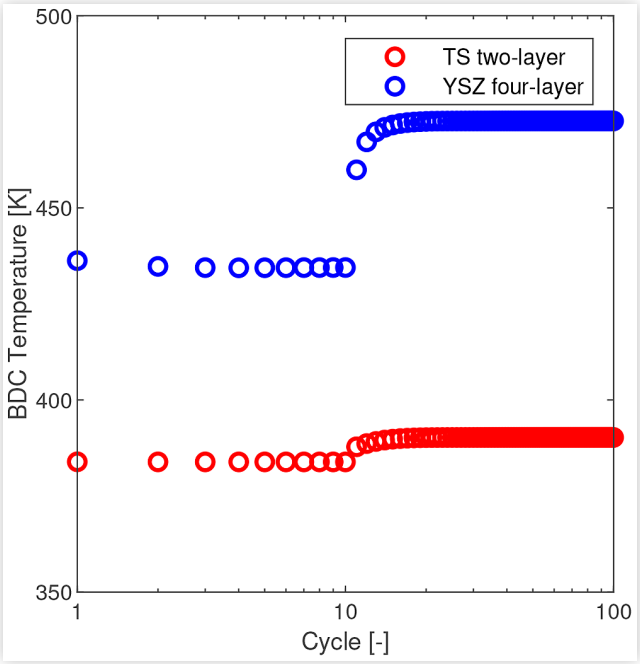

© SAE International.

The YSZ coating (blue) shows a very different response to the step change in load. Inspection of cycle 11 shows that initially and not surprisingly the wall temperature follows the history of the previous low-load cycle. At the combustion event, the higher heat flux pushes the wall temperature to a value that is close to that of cycle 100 (the nearly converged high-load condition). But, significant differences exist between cycles 11 and 100. These differences are the result of the longer 'memory' of the YSZ-coated wall seen in Fig. 3. The larger total resistance of the YSZ-coated wall results in a higher average temperature for the high load condition in comparison to the low-load condition.

Figure 7 shows results for the entire transient simulation. The temperature at the start of the compression stroke (BDC) is shown for all 100 cycles. The TS coating (red) responds in almost two cycles while the YSZ (blue) requires nearly five cycles to respond. The resulting steady state temperature difference at BDC between the low- and high-load conditions are 6 and 38K for the TS and the YSZ, respectively.

Computational Time

The proposed methodology of calculating the coated wall surface temperature can easily be implemented in any commercial engine combustion simulation software. It would only be a small part of these sophisticated codes, therefore, the important requirements are (1) low memory overhead, and (2) high computational speed/efficiency.

A time comparison was made between the proposed analytical solution and a finite-difference code. The finite difference code was initially developed to baseline the analytical model. The finite difference code used a Crank-Nicolson numerical technique, which combines Euler's method with the fully implicit method [26]. This is a popular method because it is characterized by high accuracy and stability. The present problem of a thin coating of low thermal inertia requires sufficient spatial resolution in order to fully capture the surface temperature swings. The two-layer spatial domain included 400 nodes in the TS coating and 601 nodes in the aluminum engine wall. A time-varying heat flux boundary condition was provided at the combustion chamber surface an the back-side boundary condition remained the fixed coolant temperature.

The heat flux array from the fully coupled model using the TS coated wall case was exported from the Cantera code; these results correspond to crank-angle resolved heat flux for all 100 cycles. These data were then used in a calculation of the wall surface temperature using both the analytical approach of Eq. (16) and the finite difference code. This uncoupled, standalone approach was used to isolate the wall calculations from the combustion calculations to give a more direct comparison.

The convolution (last) term of Eq. (16) requires n arithmetic operations per value of heat flux change (corresponding the size of the response factor array) and n^2 operations for n elements of the heat flux step change history (heat flux longer in the past is irrelevant because the response factor is zero) and this calculation could be extremely time consuming. The required time, however, can be significantly reduced by using fast convolution algorithms to reduce the cost of the convolution to $\mathcal{O}(n \log n)$ complexity.

The key to accessing the highest computational efficiency is the use of the fast Fourier transform (FFT) algorithm via the circular convolution theorem. More specifically, the convolution of $\Delta\dot{q}_i''$ and $g(\theta_n - \theta_i)$ is found by taking the FFT of each one, multiplying point-wise and then performing, on the product, an inverse FFT,

$$\left(\Delta\dot{q}'' * g\right)[n] = \text{ifft}\left[\text{fft}\left(\Delta\dot{q}''\right) \cdot \text{fft}\left(g\right)\right] \tag{24}$$

Figure 8 shows a comparison of the cumulative computational time for the finite difference and analytical solution. The finite difference code takes a nearly constant amount of time per cycle (~50 ms). In practice, the time per cycle could be reduced to some extent with code optimization but is fundamentally limited by the need for high spatial and temporal accuracy at the combustion chamber surface. In contrast, the analytical approach is weakly dependent on the number of cycles calculated. This is a result of the finite size of the response factor array and the FFT operation scaling discussed above. For the 100 cycle simulation, the analytic solution was found to be 200× faster than the finite difference code.

It should be noted that this speedup is for an uncoupled simulation, i.e., the heat flux time history is precomputed and used to solve for the corresponding wall temperature history. If the proposed methodology is used in a coupled simulation approach wherein the wall temperature is calculated at each time step, the computational time advantage is less significant.

Downloaded from SAE International by University of Wisconsin - Madison , Monday, July 06, 2020

FIGURE 8 Computational time required as a function of number of cycles for the finite-difference and the analytic solution

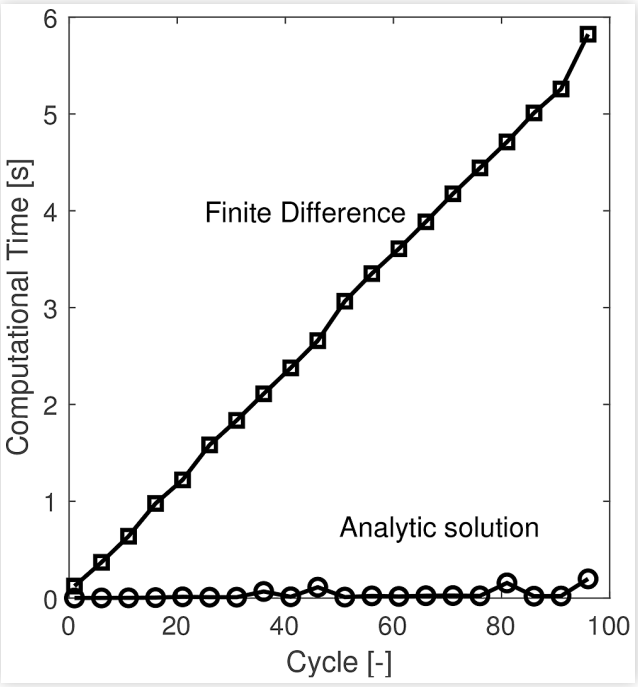

© SAE International.

Conclusions

An analytical solution for the surface temperature of a thermal barrier coated wall was developed. The major advantages of this approach are:

1. The analytical nature of the solution requires no spatial discretization and the accuracy is guaranteed.
2. Computational time is fast.
3. Any number of coating layers can be easily accommodated.

The analytical solution approach utilizes the matrix formulation that arises from Laplace transforming the heat diffusion equation. The inverse Laplace transform is performed using the residue theorem, where the poles are known to be on the negative real axis and can be found using a numerical approach. The final formulation includes a term that accounts for the water-side temperature boundary condition, another that takes into account the initial condition, a simple resistance term, and finally a convolution of the array of heat flux step changes with a response factor. The last term contains all of the coating-specific physics. This solution is an exact solution of the heat diffusion equation that relates conditions at the boundaries.

Results are demonstrated for a transient load step change calculated for 100 consecutive cycles and highlighted both the computational efficiency of the approach (a 200× speedup relative to a finite difference code for an uncoupled simulation) and the controlling physics of the wall surface temperature response.

References

1. Assanis, D., Wiese, K., Schwarz, E., and Bryzik, W., "The Effects of Ceramic Coatings on Diesel Engine Performance and Exhaust Emissions," SAE Technical Paper 910460, 1991, https://doi.org/10.4271/910460.
2. Osawa, K., Kamo, R., and Valdmanis, E., "Performance of Thin Thermal Barrier Coating on Small Aluminum Block Diesel Engine," SAE Technical Paper 910461, 1991, https://doi.org/10.4271/910461.
3. Chan, S. and Khor, K., "The Effect of Thermal Barrier Coated Piston Crown on Engine Characteristics," *Journal of Materials Engineering and Performance* 9(1):103-109, 2000.
4. Mendera, K.Z., "Effectiveness of Plasma Sprayed Coatings for Engine Combustion Chamber," SAE Technical Paper Series 1:724, 2000.
5. Schihl, P., Schwarz, E., and Bryzik, W., "Performance Characteristics of a Low Heat Rejection Direct-Injection Military Diesel Engine Retrofitted with Thermal Barrier Coated Pistons," *Journal of Engineering for Gas Turbines and Power* 123(3):644, 2001.
6. Kamo, R., Mavinahally, N.S., Kamo, L., Bryzik, W., and Schwartz, E.E., "*Injection Characteristics that Improve Performance of Ceramic Coated Diesel Engines*," 1999.
7. Dickey, D., "The Effect of Insulated Combustion Chamber Surfaces on Direct-Injected Diesel Engine Performance, Emissions and Combustion," SAE Technical Paper 890292, 1989, https://doi.org/10.4271/890292.
8. Cheng, W.K., Wong, V.W., and Gao, F., "*Heat Transfer Measurement Comparisons in Insulated and Non-Insulated Diesel Engines*," 1989.
9. Morel, T., Wahiduzzaman, S., Fort, E.F., Keribar, R., and Blumberg, P.N., "Methods for Heat Transfer and Temperature Field Analysis of the Insulated Diesel, Phase 3," Tech. Rep., NASA, 1988.
10. Havstad, P., Garwin, I., and Wade, W., "A Ceramic Insert Uncooled Diesel Engine," SAE Technical Paper 860447, 1986, https://doi.org/10.4271/860447.
11. Alkidas, A., "Performance and Emissions Achievements with an Uncooled Heavy-Duty, Single-Cylinder Diesel Engine," SAE Technical Paper 890144, 1989, https://doi.org/10.4271/890144.
12. Miyairi, Y., Matsuhisa, T., Ozawa, T., Oikawa, H. et al., "Selective Heat Insulation of Combustion Chamber Walls for a DI Diesel Engine with Monolithic Ceramics," SAE Technical Paper 890141, 1989, https://doi.org/10.4271/890141.
13. Gatowski, J., "Evaluation of a Selectively-Cooled Single-Cylinder 05-L. Diesel Engine," SAE Technical Paper 900693, 1990, https://doi.org/10.4271/900693.
14. Alkidas, A.C., "*Experiments with an Uncooled Single-Cylinder Open-Chamber Diesel*," 1987.
15. Woschni, G., Spindler, W., and Kolesa, K., "Heat Insulation of Combustion Chamber Walls - A Measure to Decrease the Fuel Consumption of I.C. Engines?" SAE Technical Paper 870339, 1987, https://doi.org/10.4271/870339.
16. Furuhama, S. and Enomoto, Y., "*Heat Transfer into Ceramic Combustion Wall of Internal Combustion Engines*," 1987.

Downloaded from SAE International by University of Wisconsin - Madison , Monday, July 06, 2020

17. Hendricks, T. and Ghandhi, J., "Estimation of Surface Heat Flux in IC Engines Using Temperature Measurements: Processing Code Effects," *SAE Int. J. Engines* 5(3):1268-1285, 2012, https://doi.org/10.4271/2012-01-1208.
18. Huang, J.C. and Borman, G.L., "Measurements of Instantaneous Heat Flux to Metal and Ceramic Surfaces in a Diesel Engine," 1, 1987.
19. Assanis, D.N., "The Effect of Thin Ceramic Coatings on Petrol Engine Performance and Emissions," *International Journal of Vehicle Design* 13(4):378-387, 1992.
20. Caputo, S., Millo, F., Boccardo, G., Piano, A., Cifali, G., and Concetto Pesce, F., "Numerical and Experimental Investigation of a Piston Thermal Barrier Coating for an Automotive Diesel Engine Application," Applied Thermal Engineering, 2019.
21. Rakopoulos, C.D. and Giakoumis, E.G., "*Study of the Transient Operation of Low Heat Rejection Turbocharged Diesel Engine Including Wall Temperature Oscillations*," 2007.
22. Kosaka, H., Wakisaka, Y., Nomura, Y., Hotta, Y.et al., "Concept of "Temperature Swing Heat Insulation" in Combustion Chamber Walls, and Appropriate Thermo-Physical Properties for Heat Insulation Coat," *SAE Int. J. Engines* 6(1):142-149, 2013, https://doi.org/10.4271/2013-01-0274.
23. Kawaguchi, A., Iguma, H., Yamashita, H., Takada, N. et al., "Thermo-Swing Wall Insulation Technology; - A Novel Heat Loss Reduction Approach on Engine Combustion Chamber," SAE Technical Paper 2016-01-2333, 2016, https://doi.org/10.4271/2016-01-2333.
24. Durrett, R.P., Najt, P.M., Andruskiewicz, P.P. IV, Schaedler, T.A., Hill, G.P., Martin, J.H., and Ro, C.J., "*Internal Combustion Engine and Method for Coating Internal Combustion Engine Components*," 2018.
25. Andrie, M., Kokjohn, S., Paliwal, S., Kamo, L. et al., "Low Heat Capacitance Thermal Barrier Coatings for Internal Combustion Engines," SAE Technical Paper 2019-01-0228, 2019, https://doi.org/10.4271/2019-01-0228.
26. Nellis, G.F. and Klein, S., *Heat Transfer* (Cambridge University Press, 2009).
27. Assanis, D.N. and Heywood, J.B., "Development and Use of a Computer Simulation of the Turbocompounded Diesel System for Engine Performance and Component Heat Transfer Studies," 1986.
28. Wong, V., Bauer, W., Kamo, R., Bryzik, W. et al., "Assessment of Thin Thermal Barrier Coatings for I.C. Engines," SAE Technical Paper 950980, 1995, https://doi.org/10.4271/950980.
29. Caputo, S., Millo, F., Cifali, G., and Pesce, F., "Numerical Investigation on the Effects of Different Thermal Insulation Strategies for a Passenger Car Diesel Engine," *SAE Int. J. Engines* 10(4):2154-2165, 2017, https://doi.org/10.4271/2017-24-0021.
30. Yao, M., Ma, T., Wang, H., Zheng, Z. et al., "A Theoretical Study on the Effects of Thermal Barrier Coating on Diesel Engine Combustion and Emission Characteristics," *Energy* 162:744-752, 2018.
31. Poubeau, A., Vauvy, A., Duffour, F., Zaccardi, J.-M., de Paola, G., and Abramczuk, M., "Modeling Investigation of Thermal Insulation Approaches for Low Heat Rejection Diesel Engines Using a Conjugate Heat Transfer Model," *International Journal of Engine Research*, 20, 1, 92-104, 2018.
32. Killingsworth, N., Powell, T., O'Donnell, R., Filipi, Z. et al., "Modeling the Effect of Thermal Barrier Coatings on HCCI Engine Combustion Using CFD Simulations with Conjugate Heat Transfer," SAE Technical Paper 2019-01-0956, 2019, https://doi.org/10.4271/2019-01-0956.
33. Rakopoulos, C., Rakopoulos, D., Mavropoulos, G., and Giakoumis, E., "Experimental and Theoretical Study of the Short Term Response Temperature Transients in the Cylinder Walls of a Diesel Engine at Various Operating Conditions," *Applied Thermal Engineering* 24(5-6):679-702, 2004.
34. Pipes, L.A., "Matrix Analysis of Heat Transfer Problems," *Journal of the Franklin Institute* 263(3):195-206, 1957.
35. Jaeger, J.C. and Carslaw, H.S., "*Conduction of Heat in Solids*," 1959.
36. Churchill, R.V. and Brown, J.W., *Complex Variables and Applications* Eighth Edition (McGraw-Hill, 2009).
37. Koutsakis, G., Nellis, G.F., and Ghandhi, J.B., "Surface Temperature of a Multi-Layer Thermal Barrier Coated Wall Subject to an Unsteady Heat Flux," International Journal of Heat and Mass transfer, 2020 (submitted).
38. Hittle, D.C. and Bishop, R., "An Improved Root-Finding Procedure for Use in Calculating Transient Heat Flow Through Multilayered Slabs," *International Journal of Heat and Mass Transfer* 26(11):1685-1693, 1983.
39. Gingrich, E., Tess, M., Korivi, V., Schihl, P., Saputo, J., Smith, G., Sampath, S., and Ghandhi, J.B., "The Impact of Piston Thermal Barrier Coating Roughness on High-Load Diesel Operation," *International Journal of Engine Research*, 2019 (accepted).
40. Overbye, V.D., Bennethum, J.E., Uyehara, O.A., and Myers, P.S., "Unsteady heat Transfer in Engines," *SAE Transactions* 69:461-494, 1961.
41. Goodwin, D.G., Speth, R.L., Moffat, H.K., and Weber, B.W., "*Cantera: An Object-Oriented Software Toolkit for Chemical Kinetics, Thermodynamics, and Transport Processes*," 2018, Version 2.4.0.
42. Ra, Y. and Reitz, R.D., "A Reduced Chemical Kinetic Model for ic Engine Combustion Simulations with Primary Reference Fuels," *Combustion and Flame* 155(4):713-738, 2008.
43. Annand, W.J.D., "Heat Transfer in the Cylinders of Reciprocating Internal Combustion Engines," *Proceedings of the Institution of Mechanical Engineers* 177(1):973-996, 1963.
44. Borman, G. and Nishiwaki, K., "Internal-Combustion Engine Heat Transfer," *Progress in Energy and Combustion Science* 13(1):1-46, 1987.

Contact Information

G. Koutsakis
Engine Research Center
University of Wisconsin-Madison
koutsakis@wisc.edu

Downloaded from SAE International by University of Wisconsin - Madison , Monday, July 06, 2020

Acknowledgments

Support for this work was provided by John Deere & Company.

Definitions, Acronyms, Abbreviations

$\dot{q}''$ - Heat Flux [Wm^{-2}]
h - Heat transfer coefficient [$Wm^{-2}K^{-1}$]
t - Temperature [K]
θ - Time [s]
k - Thermal conductivity [$Wm^{-1}K^{-1}$]
ρ - Density [kgm^{-3}]
c - Specific heat capacity [$Jkg^{-1}K^{-1}$]
ρ**c** - Volumetric heat capacity [$Jm^{-3}K^{-1}$]
x - Distance [m]
L - Length [m]
A,B,C,D - Matrix coefficients
R - Thermal resistance [m^2KW^{-1}]
C - Capacitance per unit area [$Jm^{-2}K^{-1}$]
s - Laplace, frequency variable [Hz]
β - Positive real number and simple root of D(s) [Hz]

Subscripts

g - gas
w - wall
c - coolant
m - root index

Abbreviations

TBC - Thermal Barrier Coating
YSZ - Yttria Stabilized Zirconia
TS - Thermal-swing
TDC - Top Dead Center
BDC - Bottom Dead Center
IVC - Intake Valve Closing
EVO - Exhaust Valve Opening

APPENDIX

This appendix presents the first 15 roots of D(s) required for the calculations given in the body of the paper.

TABLE 3 First fifteen roots $-\beta_m$ of the two- and four-layer test cases

	Two-layer			Four-layer		
m	$-\beta_m$	$B\|_{s=-\beta_m}$	$\frac{dD(s)}{ds}\|_{-\beta_m}$	$-\beta_m$	$B\|_{s=-\beta_m}$	$\frac{dD(s)}{ds}\|_{-\beta_m}$
1	-4.49	$+2.610 \times 10^{-5}$	$+1.70 \times 10^{-2}$	-4.47	$+4.222 \times 10^{-5}$	$+11.13 \times 10^{-2}$
2	-40.35	-1.090×10^{-5}	-0.45×10^{-2}	-13.53	-19.688×10^{-5}	-5.77×10^{-2}
3	-111.64	$+1.190 \times 10^{-5}$	$+0.15 \times 10^{-2}$	-45.13	$+0.816 \times 10^{-5}$	$+5.36 \times 10^{-2}$
4	-204.10	-7.870×10^{-5}	-0.03×10^{-2}	-110.77	-3.521×10^{-5}	-1.38×10^{-2}
5	-233.72	$+5.290 \times 10^{-5}$	$+0.03 \times 10^{-2}$	-131.70	$+1.678 \times 10^{-5}$	$+1.28 \times 10^{-2}$
6	-367.67	-0.609×10^{-5}	-0.09×10^{-2}	-242.47	-0.406×10^{-5}	-2.03×10^{-2}
7	-547.19	$+0.287 \times 10^{-5}$	$+0.13 \times 10^{-2}$	-326.58	$+4.284 \times 10^{-5}$	$+1.23\times 10^{-2}$
8	-763.21	-0.198×10^{-5}	-0.13×10^{-2}	-406.94	-0.381×10^{-5}	-1.31×10^{-2}
9	-1015.26	$+0.175 \times 10^{-5}$	$+0.11 \times 10^{-2}$	-588.51	$+0.643 \times 10^{-5}$	$+0.67\times 10^{-2}$
10	-1302.93	-0.198×10^{-5}	-0.08×10^{-2}	-649.72	-1.648×10^{-5}	-0.61×10^{-2}
11	-1624.53	$+0.340 \times 10^{-5}$	$+0.04 \times 10^{-2}$	-841.33	$+0.248 \times 10^{-5}$	$+0.97\times 10^{-2}$
12	-1918.92	-3.450×10^{-5}	-0.01×10^{-2}	-1024.23	-1.677×10^{-5}	-0.56×10^{-2}
13	-2017.59	$+1.310 \times 10^{-5}$	$+0.01 \times 10^{-2}$	-1136.92	$+0.342 \times 10^{-5}$	$+0.57\times 10^{-2}$
14	-2392.78	-0.223×10^{-5}	-0.04×10^{-2}	-1422.39	-0.360×10^{-5}	-0.47×10^{-2}
15	-2823.46	$+0.123 \times 10^{-5}$	$+0.06 \times 10^{-2}$	-1545.29	$+1.139 \times 10^{-5}$	$+0.41\times 10^{-2}$

© SAE International.

© 2020 SAE International. All rights reserved. No part of this publication may be reproduced, stored in a retrieval system, or transmitted, in any form or by any means, electronic, mechanical, photocopying, recording, or otherwise, without the prior written permission of SAE International.

Positions and opinions advanced in this work are those of the author(s) and not necessarily those of SAE International. Responsibility for the content of the work lies solely with the author(s).

e-ISSN 2641-9645